AD-A122 315 INVESTIGATION OF SMALL TRANSVERSE ELECTRIC CO2 WAVEGUIDE LASERS FOR FUZIN..(U) MARYLAND UNIV COLLEGE PARK DEPT OF ELECTRICAL ENGINEERING U HOCHULI ET AL. 1/1

UNCLASSIFIED OCT 82 HDL-CR-82-117-1 DAAG39-76-C-0117 F/G 20/5 NL

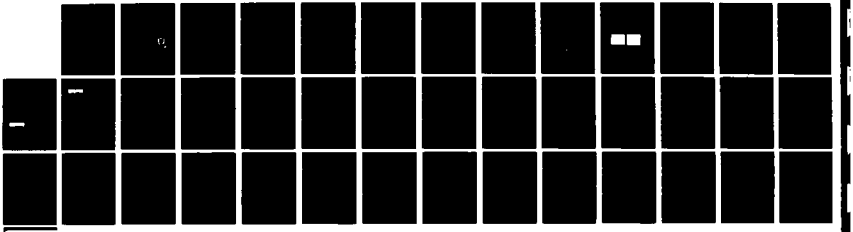

END

FILMED

DTIC

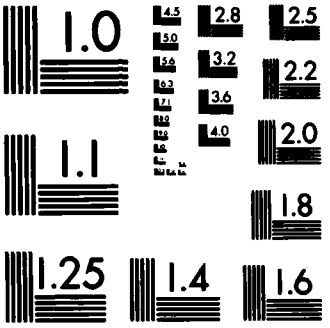

MICROCOPY RESOLUTION TEST CHART
NATIONAL BUREAU OF STANDARDS-1963-A

HDL-CR-82-117-1

October 1982

Investigation of Small Transverse Electric CO_2 Waveguide Lasers for Fuzing Applications

by Uhrs Hochuli

Prepared by

University of Maryland
Department of Electrical Engineering
College Park, MD 20784

Under contract

DAAG-39-76-C-0117

U.S. Army Electronics Research and Development Command

Harry Diamond Laboratories

Adelphi, MD 20783

The findings in this report are not to be construed as an official Department of the Army position unless so designated by other authorized documents.

Citation of manufacturers' or trade names does not constitute an official indorsement or approval of the use thereof.

Destroy this report when it is no longer needed. Do not return it to the originator.

UNCLASSIFIED

SECURITY CLASSIFICATION OF THIS PAGE (When Data Entered)

REPORT DOCUMENTATION PAGE

READ INSTRUCTIONS BEFORE COMPLETING FORM

1. REPORT NUMBER: HDL-CR-82-117-1	2. GOVT ACCESSION NO.: AD-A122 31[illegible]
3. RECIPIENT'S CATALOG NUMBER:	
4. TITLE (and Subtitle): Investigation of Small Transverse Electric CO_2 Waveguide Lasers for Fuzing Applications	5. TYPE OF REPORT & PERIOD COVERED: Contractor Report
	6. PERFORMING ORG. REPORT NUMBER:
7. AUTHOR(s): Uhrs Hochuli; HDL Contact: Dennis McGuire	8. CONTRACT OR GRANT NUMBER(s): DAAG-39-76-C-0117
9. PERFORMING ORGANIZATION NAME AND ADDRESS: University of Maryland, Department of Electrical Engineering, College Park, MD 20784	10. PROGRAM ELEMENT, PROJECT, TASK AREA & WORK UNIT NUMBERS: Program Ele: MAIF, PRON: 1A02161501GGA9
11. CONTROLLING OFFICE NAME AND ADDRESS: Harry Diamond Laboratories, 2800 Powder Mill Road, Adelphi, MD 20783	12. REPORT DATE: October 1982
	13. NUMBER OF PAGES: 40
14. MONITORING AGENCY NAME & ADDRESS (if different from Controlling Office):	15. SECURITY CLASS. (of this report): UNCLASSIFIED
	15a. DECLASSIFICATION/DOWNGRADING SCHEDULE: N/A

16. DISTRIBUTION STATEMENT (of this Report)

Approved for public release; distribution unlimited.

17. DISTRIBUTION STATEMENT (of the abstract entered in Block 20, if different from Report)

18. SUPPLEMENTARY NOTES

HDL Project: A18032
DRCMS Code: 36KA5000204

19. KEY WORDS (Continue on reverse side if necessary and identify by block number)

Carbon dioxide laser	Laser	Optical fuzing
Pulsed carbon dioxide laser	Compact carbon	Optical sensor
Carbon dioxide waveguide laser	Dioxide laser	Infrared fuzing
		Infrared sensor

20. ABSTRACT (Continue on reverse side if necessary and identify by block number)

The properties of a compact, transversely excited, pulsed CO_2 waveguide laser are studied experimentally with the application of such a laser for an optical fuze transmitter in mind. Such parameters as peak power, pulse width, pulse shape, pulse jitter, repetition rate, beam profile, polarization, laser life, and optimum gas mixture are investigated both for 10.6- and 9.6-μm output wavelengths, and for both sealed-off and flowing-gas operation of the laser. A computer simulation of the laser's operation is compared with the experimental results.

DD FORM 1 JAN 73 1473 EDITION OF 1 NOV 65 IS OBSOLETE

UNCLASSIFIED

SECURITY CLASSIFICATION OF THIS PAGE (When Data Entered)

With the flowing gas structure investigated, 200-W pulses with 60- to 120-ns half-power widths can routinely be produced, and 500-W pulses can be observed under laboratory conditions. Repetition rates up to 1 kHz can be obtained with no loss of output power, provided that gas flow rates are appropriately increased. With sealed-off operation, the main laser operation problem is to achieve useable laser lifetime at high repetition rates. The best results obtained gave a laser half-power lifetime of 120 s at a 30-Hz repetition rate. The computer-simulated operation and experimental results were in generally good agreement. Good agreement was obtained between the calculated and measured pulse rise and fall times, the width of the leading pulse, and the total energy content per pulse. Measured peak output power is generally smaller than that predicted, however. This discrepancy may be due to the single-frequency output assumption in the computer model.

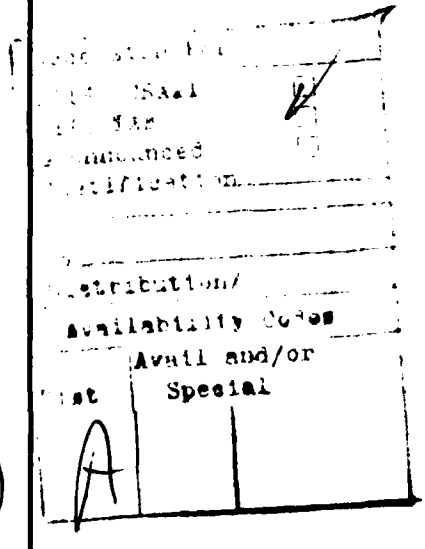

CONTENTS

FIGURES

FIGURES (Cont'd)

1. INTRODUCTION

The CO_2 waveguide laser is a potential component for active optical fuze systems that offer several advantages over present technology. These advantages include high average power, high degrees of coherence and polarization, and potentially greatly improved performance in fog and cloud environments compared to GaAs systems.

Recent experimental studies[1,2] indicate that a pulsed, transverse electric CO_2 waveguide laser developed for fuzing applications is capable of peak powers in excess of 100 W and pulse widths less than 200 ns. These results were obtained with a compact sealed-off structure, having a total length of 12.7 cm and rigidly attached mirrors, and requiring no angular or longitudinal tuning adjustments. Pulse repetition rates were low, however, being about 10 Hz. It is known that peak pulse power decreases at high repetition rates and asymptotically approaches the cw situation where roughly 1 W of output can be expected.

To be useful in a fuzing application, the laser must be operated at higher repetition rates and with shorter pulses to meet resolution and encounter scenario requirements. Goals in this regard are for repetition rates of tens of kilohertz (although a few kilohertz could be useful) and for pulse widths of about 20 ns (here, too, somewhat greater pulse widths could be useful). Operating lifetimes of the laser, as opposed to shelf life, need not be very great, however. A laser capable of functioning reliably for as little as 10 s could be useful, although several minutes of function life would widen its area of applicability significantly.

The research reported herein is an experimental and theoretical investigation of the extent to which the goals outlined above could be achieved with the laser structure in question. The relative merits of sealed-off versus flowing gas systems in meeting the repetition rate and lifetime goals were investigated in particular, and computer studies and careful pulse shape measurements were used to determine to what extent the pulse width goal can be met.

---

[1] *P. W. Smith, P. J. Maloney, and O. R. Wood, II, Waveguide TEA Laser, Appl. Phys. Lett. 23 (1973), 524.*

[2] *U. Hochuli, Properties of Small TE CO_2 Waveguide Lasers, Dept. of Electrical Engineering, University of Maryland, Technical Research Report for Contract No. DAAG30-76-C-0117, Contract report for Harry Diamond Laboratories, HDL-CR-77-117-1 (June 1977).*

2. EXPERIMENTAL DETAILS

2.1 Laser Construction

The basic laser structure consists essentially of a beryllia U channel containing 51 copper cathode pin electrodes and a flat copper plate acting as an anode and heat sink. The square bore measures 1 mm on a side and is 12.7 cm long, with the cathode pins evenly distributed along the central 10 cm of the bore. Such a structure, together with the fact that it can be made to lase without any mirror tuning, lends itself well to metal-ceramic construction with solder seals.

We initially used a sealed structure of this type and later found that it was quite difficult to clean the products of sputtering from its closed bore. These sputtering products greatly increase the losses of the waveguide, resulting in a pulse delay increase from about 1 μs for a clean bore to about 2 μs for a dirty bore. Pulse delay is here defined as the time interval between onset of electrode discharge current and start of laser output. The mentioned increase of the waveguide losses reduces of course the available laser output as well. In order to avoid the cleaning problems of a sealed bore, we have designed and used the structure shown in figure 1, which is easily disassembled and lends itself better to experimental changes.

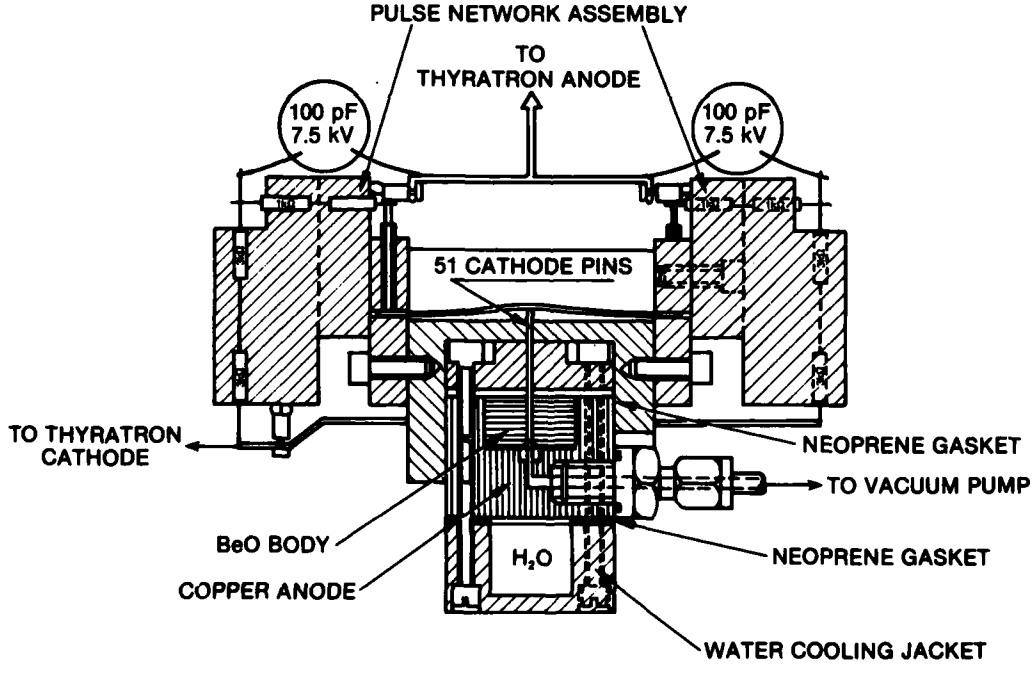

Figure 1. Cross section of demountable laser structure.

2.2 Laser Excitation Circuitry

Standard hydrogen thyratron circuitry as shown in figure 2 was used to charge and discharge the 51 energy storage capacitors (100 pF each) feeding the laser electrodes. The corresponding voltage and current waveforms are shown in figure 3.

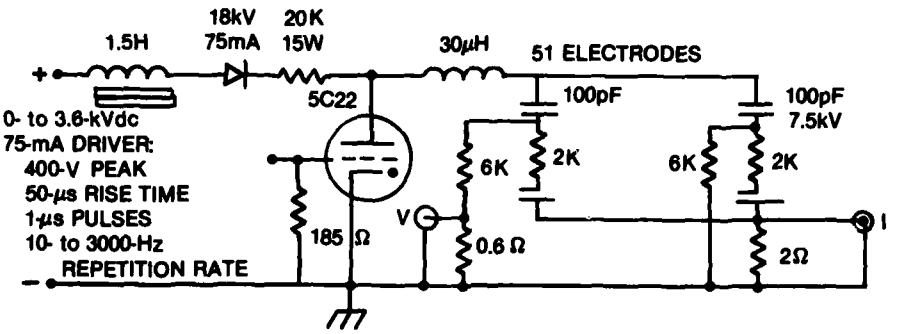

Figure 2. Electrical pulse circuit.

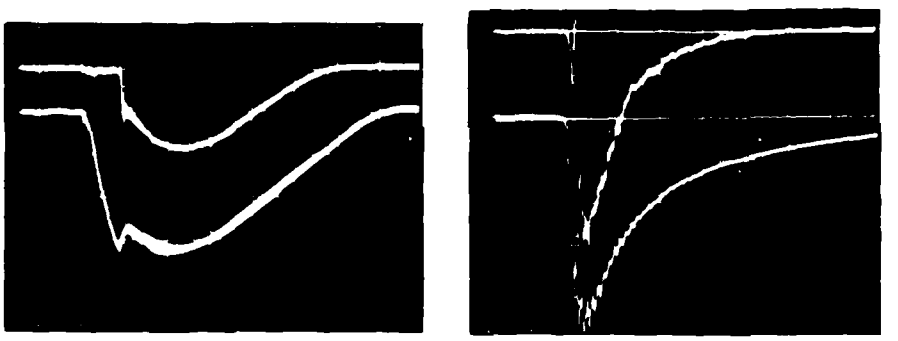

Figure 3. Current and voltage waveforms. Upper traces: 10 A and 200 ns per div. Lower traces: 500 V and 200 ns per div. Right picture: 30-μH coil shorted.

The circuit works satisfactorily up to the 3-kHz repetition rate desired for the laser. Repetition rates up to 5 kHz are possible, but cannot be handled efficiently by the laser structure due to its longitudinal flow resistance and to the turbulence problems associated with the rapid flow required. Polarization losses in the 100-pF ceramic

disc capacitors produce considerable heating at repetition rates as low as 1 kHz. The capacitors were air-cooled for continuous laser operation at 1-kHz repetition rates or above.

It should be noted that the 15-W 20-kΩ resistor in the 5C22 anode path limits the thyratron current if the thyratron stays on. At the same time, this resistor dampens the charging circuit and allows the 100-pF capacitors to be charged only to the power supply voltage. This kind of inefficiency can be tolerated in the laboratory, but certainly not in a portable unit. For field use, a considerable effort would have to go into the design of an efficient, practical, small, and lightweight pulse power supply. With this fact in mind we did not try to apply more than 3.6 kV to the 51 energy storage capacitors.

2.3 Gas Flow Control

In order to maintain the proper gas mixture ratios over a wide range of flow rates, we were forced to calibrate and monitor the flow rates of the individual components, He, CO_2 and N_2, of the gas mixture. The calibration curves for the Brooks R-2-15-A, -AA, and -AAA flow tubes with the appropriate floats are shown in figure 4. Once the proper gas mixture has been established, premixed gas with a single flow-control valve can be used to feed the laser.

2.4 Measuring Techniques

We used a Laser Precision RK3232 energy meter to measure pulse energies. Accurate peak power measurements are more difficult to make. They require either accurate pulse shape information to convert the pulse energy to peak power or calibrated peak power detectors with a fast response time. We used Molectron P5-00 and P3-01 calibrated pyroelectric detectors to measure the peak power. The rise times of the P5-00 detector, HP462A preamplifier, and Tektronix 7844 oscilloscope used are 0.5, 4, and 0.8 ns, respectively. An antireflection-coated Ge lens with a focal length of 25 mm was used to concentrate all the beam power on the 1-mm^2 sensitive detector area. Piezoelectric ringing around 2.5 MHz did not allow us to make meaningful measurements of the pulse tail with this type of detector. Instead, we used a Santa Barbara Research Center Model 9879 Ge:Au detector for these measurements. The rise time of this detector is 50 to 100 ns, the fall time 100 to 200 ns. Despite the fact that we carefully tried to stay within Molectron's published detector overload characteristics, two P5-00 detectors were destroyed by crystal cleavage. The P3-00 suffered no such damage.

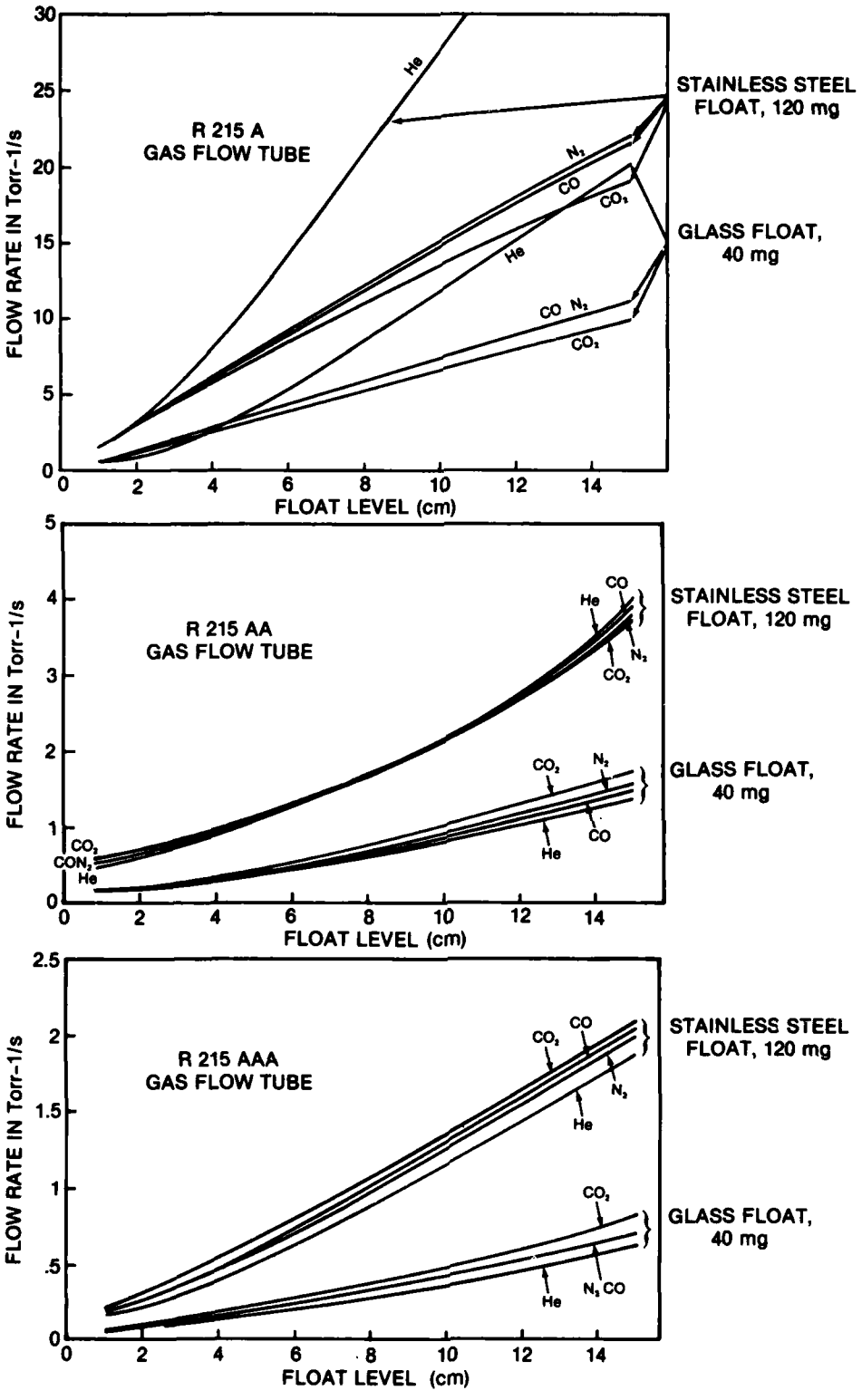

Figure 4. Flow rates versus float level for R215A, AA, and AAA flow tubes.

3. EXPERIMENTAL RESULTS

3.1 Pulse Power and Energy

Laser mirror alignment for shortest pulse delay corresponds closely to the He-Ne laser prealignment mirror positions. Such an alignment usually does not correspond to maximum peak power output. Careful alignment for maximum peak power allows us to extract about 1.5 times the minimum-delay power. This alignment is quite critical and probably represents an optimum match between the optical beam geometry and the particular spatial discharge configuration at the time of measurement. The maximum peak power is, in our judgement, an experimental laboratory value indicating the potential of the device rather than a practical, easily achievable tuning adjustment. The curves in figure 5 show the maximum peak power and the minimum-delay pulse power versus output coupling. The shaded area indicates the range of minimum-delay pulse power variations for cavity length changes from L to L + $\lambda/2$. The maximum power adjustment is even more sensitive to cavity length tuning. It is not unusual to observe power drops into the lower range of the shaded area for such tuning.

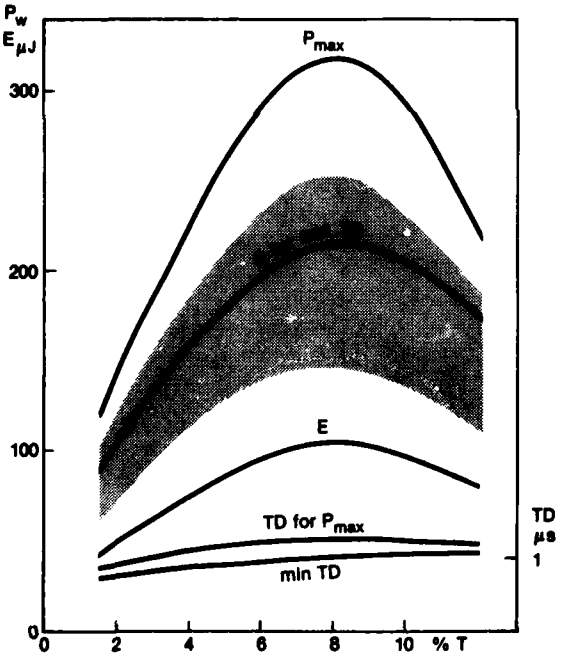

Figure 5. Maximum power, minimum-delay power, energy, and time delay versus mirror transmission. Shaded area indicates minimum-delay power variations for cavity length tuning.

Figure 5 also shows the pulse energy versus output coupling. Surprisingly, the pulse energy is practically the same for the two different mirror adjustments. The minimum-delay adjustment results in a pulse shape with less energy in the leading pulse and more energy in the pulse tail than results from the maximum power adjustment.

3.2 Pulse Delay

The pulse delay is a good indication of the net gain of the laser structure. Typical delay times for clean structures with output coupling $\lesssim 6$ percent are about 1 μs. A dirty waveguide or larger output coupling leads to delay times up to 2 μs. Delay times were measured from the onset of the discharge current to onset of the leading edge of the output pulse. Typical delay times versus output coupling are also shown in figure 5.

3.3 Pulse Shape

The half-power pulse width of the leading peak is about 60 to 120 ns. Low output coupling yields a fast rise time and a slower decay rate, while a large output coupling increases the rise time and shortens the decay time. These results agree with Casperson's[3] approximations and the results of the more sophisticated computer model discussed later. Typical pulse shapes for minimum pulse delay tuning as observed with three different detectors are shown in figure 6. Figure 7(a) shows the pulse shape if the laser is tuned for maximum power output. Figures 7(b) and 7(c) display 1000 consecutive pulses and indicate the pulse jitter. The major part of this jitter comes from pulse-to-pulse gain variations in the laser itself and not from the thyratron and gas breakdown conditions. These gain variations are probably due to spatial variations of the discharge patterns for the 51 laser electrodes.

(a) Ge:Au (b) P3-01 (c) P5-00

Figure 6. Pulse shapes with different detectors: 500 ns per div., 1000 pps, He:CO_2:N_2 4:2:1, 280 Torr, 20 Torr ℓ/s; mirror reflectivity, R = 0.94, minimum delay adjustment. (Note piezoelectric ringing of pyroelectric P3-01 and P5-00 detectors.) Discharge current waveform is shown in top traces.

[3] *Lee W. Casperson, Analytic Modeling of Gain-Switched Lasers, Laser Oscillators, J. Appl. Phys. 43 (1976), 4555.*

Figure 7. Pulse shapes and jitter: (a) maximum power adjustment, same parameters as for figure 6, Ge:Au detector. (b) 100 ns per div., P5-00 detector, 1000 pps; 1-s exposure indicates pulse jitter. (c) 30-μH coil in pulse circuit shorted out. 100 ns per div., P5-00 detector, 1000 pps; 1-s exposure indicates pulse jitter. Same discharge current waveform as shown in figure 3. Other parameters in (b) and (c) are same as for figure 6. Ringing preceding laser pulse in (c) is due to unwanted coupling from discharge circuit.

The pulse tail occurs because of gain recovery through laser ground state decay and continuing collisional energy transfer from vibrationally excited N_2. Reducing the N_2 content of the gas mixture reduces the pulse tail together with the power output. If our pulse height and energy measurements are correct, we have to conclude that the pulse tail contains considerably more energy than does the leading pulse for our gas mixture, which was optimized for maximum power output.

3.4 Pulse Spectrum

In order to suppress the 9.6-μm laser output, all our output mirrors were coated for a transmission of at least 10 percent at 9.6 μm. Despite this precaution we have been able to observe the 9.6-μm P(16) and P(20) transitions with output mirrors of 98.5- and 96-percent reflectivity (R) at 10.6 μm. The output power in these transitions was less than 30 W.

The 10.6-μm output with mirrors of $R \leq 92$ percent at 10.6 μm is mostly due to the P(16), P(18), P(20), and P(22) lines. Tuning the cavity length from L to $L + \lambda/2$ usually produces a single transition output, with short overlap periods of increased jitter where the output switches from one line to the next. Mirrors with $R \geq 94$ percent at 10.6 μm quite often produce 10.6-μm pulses where the leading pulse contains significant output on more than one line.

The axial mode spacing for a 12.7-cm cavity is about 1170 MHz. The pressure broadening at 300 Torr yields a laser gain profile width of about 1500 MHz. This situation allows the possibility that two axial cavity modes could oscillate simultaneously. The spectrograph used could not resolve two axial modes, and no attempt was made to use a high resolution etalon or to observe the beat frequency spectrum.

3.5 Pulse Jitter

The main contribution to the pulse jitter occurs from variations in the laser delay time from pulse to pulse. Figure 7(b) shows the overlap of 1000 consecutive pulses and indicates jitter about a pulse width under this condition. Shorting out the 30-μH coil in the pulse circuit reduces the jitter as shown in figure 7(c). This result is caused by a faster gain rise at the threshold level and perhaps a spatially more uniform discharge distribution as a result of harder plasma excitation.

3.6 Repetition Rate

Pulse power increases with gas flow rate until the whole bore volume is refilled with fresh gas for each pulse. Figure 8 shows that, up to 1-kHz repetition rates, no decrease in output power occurs if the gas flow rate is adjusted accordingly. At higher repetition rates, the gas flow rates become excessive for longitudinal flow. Turbulence effects increase the jitter, the pressure drops across the laser, and power input and electrode erosion all become excessive. At 3 kHz, half the power drop at the fastest flow rate is due to a lower voltage buildup across the energy storage capacitors.

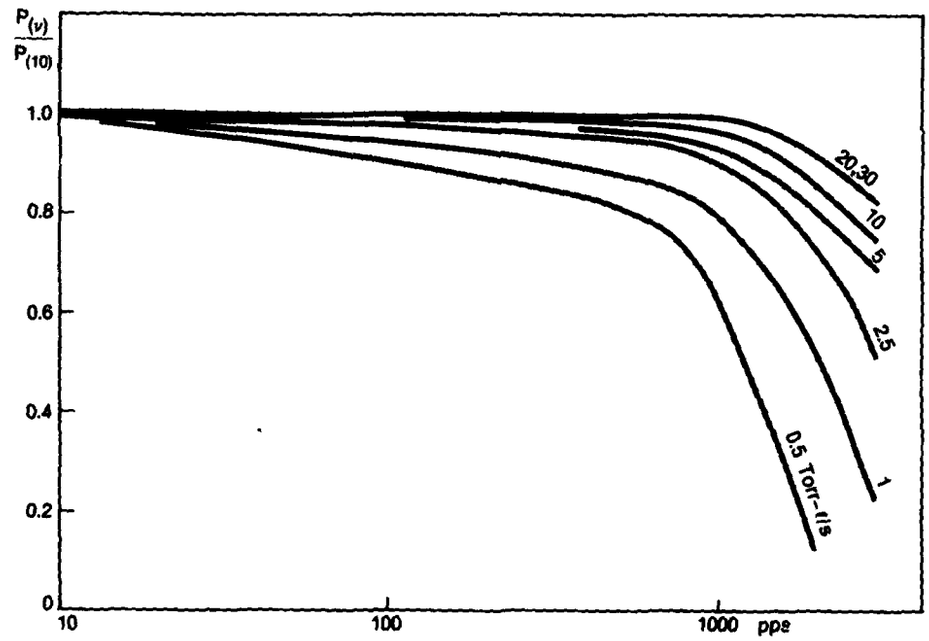

Figure 8. Output power versus repetition rate (1 Torr-ℓ/s = 40 bore volumes/s).

3.7 Warmup Transient

Other than length detuning due to heating, we have not observed any power output fluctuations. If the laser cavity is kept tuned during warmup, no power output change takes place. Lack of such tuning leads, of course, to the same power output variations as the ones caused by cavity length changes from L to L + $\lambda/2$. This observation holds for our structure with a 20 C water-cooled heat sink, pulse repetition rates below 3 kHz, and discharge conditions with well "burned-in" electrodes. It is not known whether an extended shelf storage would require a new burn-in procedure to reach stable discharge conditions.

3.8 Beam Profile and Polarization

The vertical and horizontal beam profiles, measured 1.4 m from the laser, are shown in figure 9. These profiles closely agree with theoretical predictions.

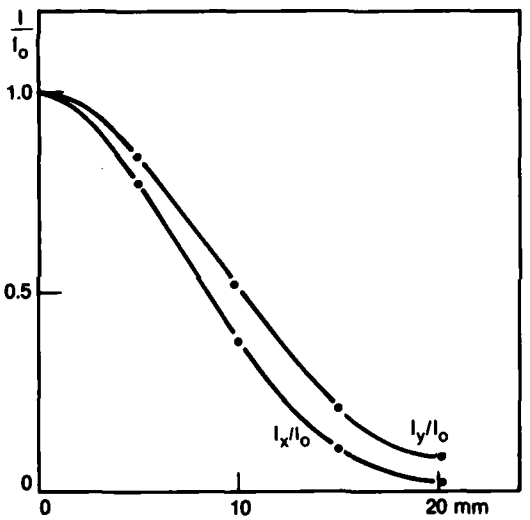

Figure 9. Beam profile 1.4 m from laser.

The electric field vector of the beam is parallel to the copper anode, and the power ratio of the orthogonally polarized outputs is about 50 to 1.

3.9 Optimum Gas Mixture

The definition of an optimum mixture is a difficult one. It is possible to maximize the power output, or minimize the jitter, or perhaps minimize the sputtering products, by adjusting the composition of the gas mixture. It can generally be said that He-rich mixtures break down somewhat easier and allow the laser to work at higher pressure with reduced jitter.

Figure 10 shows that the highest power can be obtained with an $He:CO_2:N_2$ 4:2:1 mixture. The 7:3:1 mixture yields slightly less power with a smaller variation over a wider pressure range. It also works with less jitter at high pulse repetition rates.

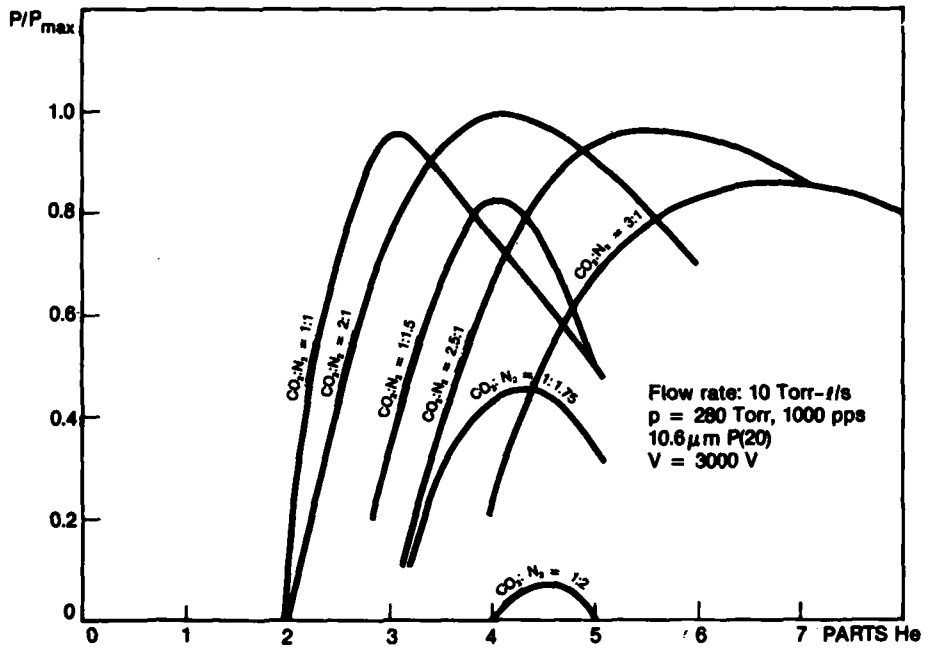

Figure 10. Power output for different gas mixtures.

3.10 Laser Life

Typical curves of laser output power versus time at a repetition rate of 1 kHz are shown in figure 11. These curves indicate that it takes about 1 hour to burn in the electrodes. Flat electrodes seem to produce the smallest waveguide losses and the largest power output. After 8 to 10 hours the power output is reduced to about 70 percent. Inspection of the channel reveals that sputtering products have accumulated and cathode pin erosion is visible. Cleaning the laser and life testing again show that the original curve is repeated but the maximum power output reached after about 2 hours is lower. This is probably due to higher waveguide losses from eroded cathode pins.

We have tried to avoid cathode edge erosion by drilling 0.3-mm holes in the centers of the 1-mm cathode pins. This process also results in higher waveguide losses and a lower output power as shown by the corresponding curve.

Flat but 0.2-mm recessed cathode pins show the highest waveguide losses. The life of such a laser seems to be longer because electrode deposits around the recessed electrodes are not as visible to the waveguide. The power dip that occurs after between 2 and 5 hours may be caused by the time-dependent spatial burn-in pattern of the electrodes.

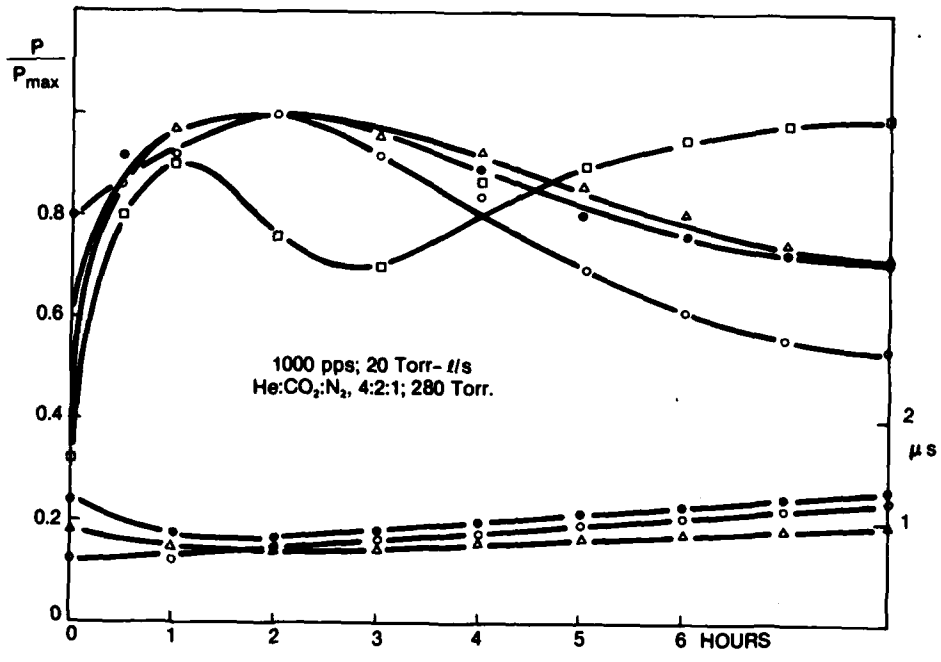

Figure 11. Power output and pulse delay versus laser life:
Δ, flat electrodes, P_{max} = 155 W, R = 0.96,
●, 0.3-mm holes in electrodes, P_{max} = 125 W, R = 0.96,
□, 0.2-mm recessed electrodes, P_{max} = 100 W, R = 0.96, and
o, flat electrodes, 30 μH shorted, P_{max} = 220 W, R = 0.94.

Omission of the 30-μH coil in the discharge path doubles the discharge current peak and leads to faster cathode erosion and shorter life, as shown by the last curve.

3.11 Output Power at 9.6 μm

Power output in the 9.6-μm band is roughly similar to the 10.6-μm output. If a Ge:Au detector is used for these measurements we have to consider the frequency response of this type of detector. Typical sensitivities are 4 to 5 times higher at 9.6 μm than at 10.6 μm. Lack of a set of mirrors with the proper reflectivities prevented us from making detailed measurements.

4. COMPUTER SIMULATION

4.1 Computer Model

The excitation mechanism of the CO_2 laser consists of electrons transferring their energy to the vibrational states of the CO_2 and N_2 molecules. These vibrational modes in turn relax through molecular collisions and one of the intravibrational transitions generates the 10.6-μm laser oscillation.

There are three vibrational modes for the CO_2 molecule: the asymmetric stretching mode (ASM), the symmetric stretching mode (SSM), and the bending mode (BM); the diatomic N_2 molecule has only one vibrational mode (NVM). The energy-level diagram is shown in figure 12.

The time evolution of the energy stored in these vibrational modes, the translational temperature,[4-6] and the laser cavity intensity are described by a set of six nonlinear coupled differential equations, equation 1 (a to f). These equations are based on the following assumptions.[5,6]

(a) All vibrational modes are purely harmonic and each is in local Boltzmann equilibrium due to rapid intramode vibrational-vibrational energy transfer; they are each described by their vibration temperature, T_i, and mode energy, E_i.

(b) Translation and rotation are tightly coupled and their distribution in energy space can be described by the kinetic temperature, T.

(c) Throughout this whole discussion, single-frequency resonance is assumed.

(d) Transverse beam intensity variations are neglected.

---

[4] *W. J. Witteman, On Vibrational Relaxations in Carbon Dioxide, Philips Res. Rep., Suppl. 2 (1963).*

[5] *K. R. Manes and H. J. Seguin, Analysis of the CO_2 TEA Laser, J. Appl. Phys. 43 (1972), 5073.*

[6] *D. L. Lyon, Comparison of Theory and Experiment for a Transversely Excited High-Pressure CO_2 Laser, IEEE J. Quantum Electron. QE-9 (1973), 139.*

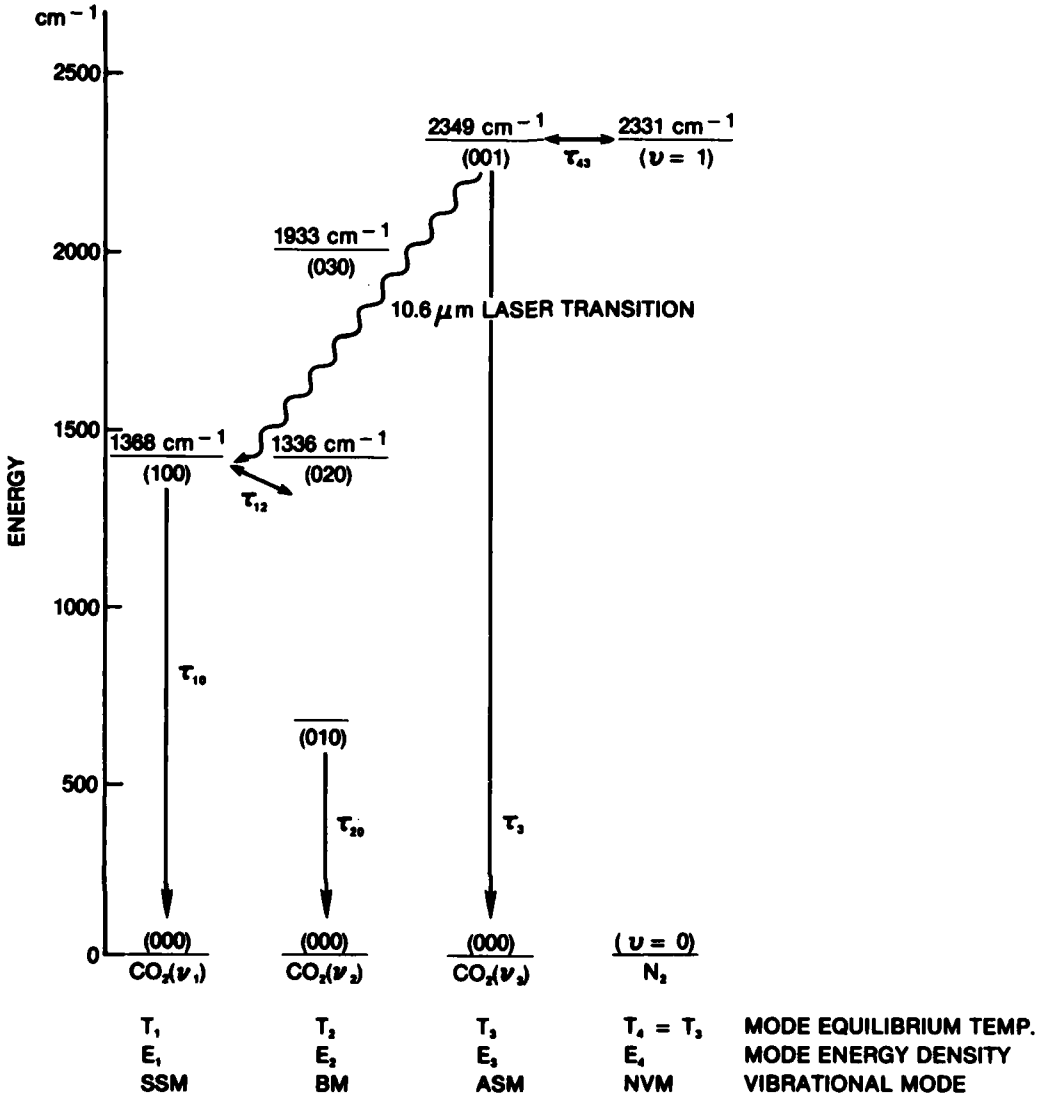

Figure 12. CO_2-N_2 molecular energy diagram.

Equation 1 (a to f) follows.

$$\frac{dE_1}{dt} = F_1(t) - \frac{E_1 - E_1^e(T)}{\tau_{10}(T)} - \frac{E_1 - E_1^e(T_2)}{\tau_{12}(T_2)} + \frac{\nu_1}{\nu_3}\frac{E_3 - E_3^e(T,T_1,T_2)}{\tau_3(T,T_1,T_2)} + h\nu_1 \Delta NWI \qquad (1a)$$

$$\frac{dE_2}{dt} = F_2(t) + \frac{E_1 - E_1^e(T_2)}{\tau_{12}(T_2)} - \frac{E_2 - E_2^e(T)}{\tau_{20}(T)} + \frac{\nu_2}{\nu_3}\frac{E_3 - E_3^e(T,T_1,T_2)}{\tau_3(T,T_1,T_2)} \quad , \tag{1b}$$

$$\frac{dE_3}{dt} = F_3(t) - \frac{E_3 - E_3^e(T,T_1,T_2)}{\tau_3(T,T_1,T_2)} + \frac{E_4 - E_4^e(T_3)}{\tau_{43}(T_3)} - h\nu_3 \Delta NWI \quad , \tag{1c}$$

$$\frac{dE_4}{dt} = F_4(t) - \frac{E_4 - E_4^e(T_3)}{\tau_{43}(T_3)} \quad , \tag{1d}$$

$$\left(\frac{3}{2}N + N_{CO_2} + N_{N_2}\right)\frac{dkT}{dt} = \frac{E_2 - E_2^e(T)}{\tau_{20}(T)} + \frac{E_1 - E_1^e(T)}{\tau_{10}(T)} + \left(\frac{\nu_3 - \nu_1 - \nu_2}{\nu_3}\right)\frac{E_3 - E_3^e(T,T_1,T_2)}{\tau_3(T,T_1,T_2)} \quad , \tag{1e}$$

$$\frac{dI}{dt} = ch\nu_L W\left(I\Delta N + I_0 "N_2"\right) - \frac{1}{\tau_c}\left(I - I^e\right) \quad , \tag{1f}$$

where

E_i = mode energy density,

E_i^e = equilibrium value of E_i,

T_i = mode equilibrium temperature,

T = translational temperature,

F_i = $\bar{e}$ pumping rate density (excitation function),

N_{CO_2} and N_{N_2} = molecular densities,

ΔN = population inversion density,

I = cavity field intensity,

I^e = thermal equilibrium value of I,

I_0 = spontaneous radiation intensity,

ν_L = laser frequency,

W = transition rate, and

τ_c = cavity decay time.

4.2 Excitation Functions

Optimum excitation efficiency requires control of the E/N ratio. The simple pulse circuit used offers only very limited control of the excitation pulse shape. We have used the waveforms shown in figure 13 to calculate the electric field, power input, and excitation functions $F_i(t)$ by

$E = (V_d - V_c)$/electrode distance, and

$P_I = (V_d - V_c)\bar{I}$, where

V_c = cathode fall, roughly 300 V,

V_d = voltage across electrodes,

$\bar{I}$ = discharge current, and

P_I = discharge power input.

Calculations of the power transfer ratios first require a knowledge of the electron energy distribution function f(u) obtained as a solution of the simplified Boltzmann equation[7]

$$-\frac{(E/N)^2}{3} u \frac{df}{du} \left\{ \sum_j \delta_j Q_{ej} \right\}^{-1} = \sum_{jk} \delta_j \int_u^{u+u_{jk}} uf(u)\, Q_{jk}(u)\, du \quad ,$$

where

E = electric field intensity,

N = total neutral molecule density,

Q_{ej}, Q_{jk} = electron-molecule and molecule-molecule collision cross section, and

δ_j = fractional concentration of the j^{th} molecule.

---

[7] *W. L. Nighan, Electron Energy Distribution and Collision Rates in Electrically Excited N_2, CO, and CO_2, Phys. Rev. 2 (1970), 1989.*

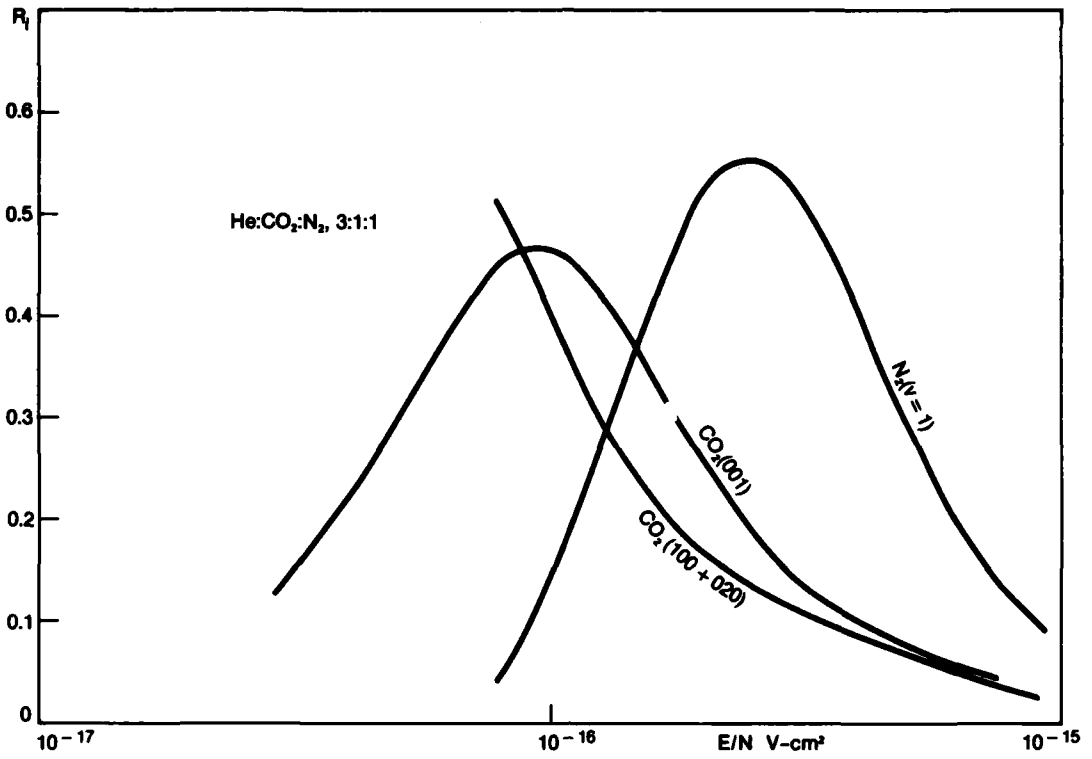

Figure 13. Excitation ratios R_i versus E/N.

The distribution function allows the collision frequencies $\bar{\nu}_{jk}$ and the electron drift velocity V_D to be calculated. The power transfer ratio R_i is now given by[7]

$$R_i = \left[eV_D E/N\right]^{-1} \sum_k \delta_i eu_{ik} \bar{\nu}_{ik}/N_i \quad .$$

The excitation function F_i is then given by

$$F_i = P_I R_i/\text{discharge volume} \quad .$$

Fortunately, Dr. W. L. Nighan of United Aircraft Research Laboratories loaned us his computer results for an $He:CO_2:N_2$ 8:1:1 gas

[7] *W. L. Nighan, Electron Energy Distribution and Collision Rates in Electrically Excited N_2, CO, and CO_2, Phys. Rev. 2 (1970), 1989.*

mixture. With the help of his collision cross sections we were able to scale his results to our 3:1:1 gas mixture.

The power transfer ratios obtained for the pertinent vibrational levels are shown in figure 13. Straight-line approximations of the corresponding power inputs are shown in figure 14.

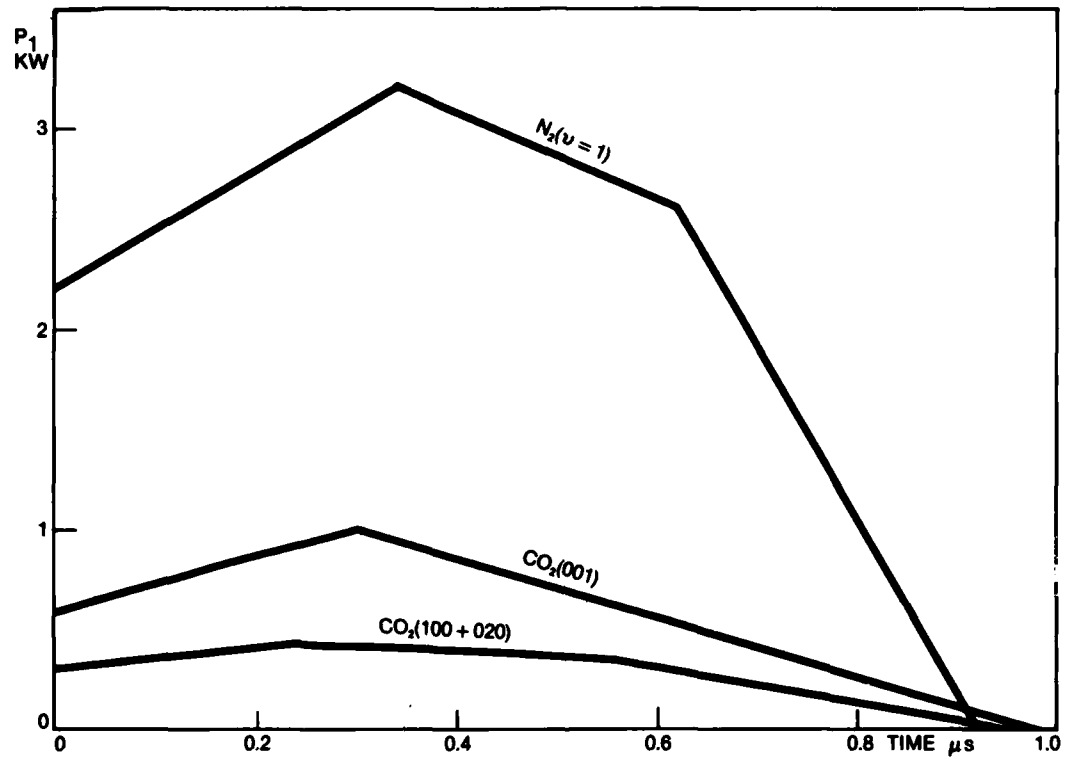

Figure 14. Vibrational mode input power versus time.

4.3 Numerical Computations

For numerical solution of the differential equations (1a through f), the various equilibrium densities, relaxation times, etc., are obtained as follows. Defining

$$y_1^{-1} \equiv N_{CO_2} h\nu_1/E_1 = \exp\left(h\nu_1/kT_1\right) - 1$$

$$y_2^{-1} \equiv N_{CO_2} h\nu_2/E_2 = \exp(h\nu_2/kT_2) - 1 \quad ,$$

$$y_3^{-1} \equiv N_{CO_2} h\nu_3/E_3 = \exp(h\nu_3/kT_3) - 1 \quad ,$$

$$y_4^{-1} \equiv N_{N_2} h\nu_4/E_4 = \exp(h\nu_4/kT_4) - 1 \quad ,$$

we have,[1,2]

$$E_1^e(T) = N_{CO_2} h\nu_1 \left[\exp(1920T^{-1}) - 1\right]^{-1} \quad ,$$

$$E_1^e(T_2) = N_{CO_2} h\nu_1 \left[(1 + y_2^{-1})^2 - 1\right]^{-1} \quad ,$$

$$E_2^e(T) = N_{CO_2} 2h\nu_2 \left[\exp(960T^{-1}) - 1\right]^{-1} \quad ,$$

$$E_3^e(T,T_1,T_2) = N_{CO_2} h\nu_3 \left[(1 + y_1^{-1})(1 + y_2^{-1}) \exp(500T^{-1}) - 1\right]^{-1} \quad ,$$

$$E_4^e(T_3) = N_{N_2} h\nu_3 y_3 \quad ,$$

and[3]

$$\tau_{12}(T_2) = 1.27 \times 10^{-3} \left(2y_2 + 1\right)^{-1} \quad ,$$

$$\tau_{20}(T) = 180 \exp(10.6 - 16.35T^{-1/3}) \quad ,$$

$$\tau_3(T,T_1,T_2) = \frac{\left[1 - \exp(-1920T^{-1})\right]\exp(500T^{-1})}{120\kappa_{ab}\left[1 - \exp(-960T^{-1})\right]\left[(1 + y_1)(1 + y_2)\exp(500T^{-1}) - y_1 y_2\right]} \quad ,$$

---

[1] *P. W. Smith, P. J. Maloney, and O. R. Wood, II, Waveguide TEA Laser, Appl. Phys. Lett. 23 (1973), 524.*

[2] *U. Hochuli, Properties of Small TE CO_2 Waveguide Lasers, Dept. of Electrical Engineering, University of Maryland, Technical Research Report for Contract No. DAAG30-76-C-0117, Contract report for Harry Diamond Laboratories, HDL-CR-77-117-1 (June 1977).*

[3] *Lee W. Casperson, Analytic Modeling of Gain-Switched Lasers, Laser Oscillators, J. Appl. Phys. 43 (1976), 4555.*

$$\kappa_{ab} = \begin{cases} \exp(6.21 - 2.684T^{-1/3}) , & 300 \text{ to } 385 \text{ K} , \\ \exp(15.62 - 70.84T^{-1/3}) , & 385 \text{ to } 1000 \text{ K} , \end{cases}$$

$$\tau_{10} = 4.5\tau_{20}$$

$$\tau_c^{-1} = (L - \ln R)c/2d = 1.2 \times 10^9(2\alpha d - \ln R) ,$$

$$W = F\lambda^2/4\pi^2 h\nu_L \tau_{sp} \Delta\nu_L = 1.1 \times 10^{-3} F T^{1/2} \text{ m}^2 \text{J}^{-1} ,$$

$$\Delta N = \frac{47 N_{CO_2}}{T} \frac{y_3(1 + y_3)^{-1} \exp(-241T^{-1}) - y_1(1 + y_1)^{-1} \exp(-265T^{-1})}{(1 + y_1)(1 + y_2)^2(1 + y_3)}$$

$$\text{"}N_2\text{"} = 47 N_{CO_2} T^{-1}(1 + y_1)^{-1}(1 + y_2)^{-2}(1 + y_3)^{-2} y_3 \exp(-241T^{-1}) ,$$

$$I_0 = h\nu_L c/\text{vol} = 5 \times 10^{-5} \text{ W m}^{-2} ,$$

$$I^e = I_0 \left[\exp(1355T^{-1}) - 1\right]^{-1} ,$$

L = $2\alpha d$ fractional round-trip waveguide loss,

d = 0.127-m cavity length,

F = filling factor ≡ gain volume/cavity volume,

J = rotational quantum number, e.g., J = 20 for the P(20) line,

R = mirror reflectivity, and

N = 1.9×10^{18} cm^{-3}, total particle density corresponding to a total pressure of 270 Torr He:CO_2:N_2 3:1:1 mixture.

These values were used to solve the set of differential equations in equation 1 (a through f) with the help of a standard Runge-Kutta program available on the University of Maryland UNIVAC 1108 and 1100/43 computers.

The following four parameters were used to fit the experimental data:

αd = the fractional waveguide loss,

R = the mirror reflectivity,

F = the filling factor, and

A = the excitation parameter.

The actual excitation functions used were defined as

$$F_i^1 \equiv \frac{A}{A_{N_2}} F_i \quad \text{with}$$

$$A_{N_2} \equiv \frac{F_{N_2}}{N_{N_2} h\nu} = 0.3 \times 10^6 \ s^{-1} \ .$$

A close fit, disregarding absolute power values, to the experimental curves of power output and delay time versus mirror transmission was obtained with

$$\alpha d = 0.14, \quad F = 0.8, \quad \text{and} \quad A = 0.18 \times 10^6 \ s^{-1} \ .$$

These results, shown in figure 15, indicate maximum power output for R = 0.93. Computed pulse shapes obtained with those parameters and different mirror reflectivities are shown in figure 16. Instantaneous calculated level population densities for R = 0.94 are shown in figure 17. Figure 17 also shows the instantaneous calculated gas temperature.

4.4 Comparision between Computer and Experimental Results

As shown in figure 15, it is possible to get close agreement between the shape of the computed and measured curves by adjusting the parameters αd, A, and F. We have not, however, been able to get the correct magnitude of power output with our computer model and the available parameters. The agreement between calculated and measured rise and fall times, as well as the width of the leading pulse and the total energy content per pulse, is relatively close; the energy distribution is not. The energy content of the experimental pulse tail is always larger than the computer model predicts. As a consequence, the leading, measured pulse peak is always smaller than the computer model result. One of the weaknesses of the computer model that may be responsible for this discrepancy is the single frequency output assumption.

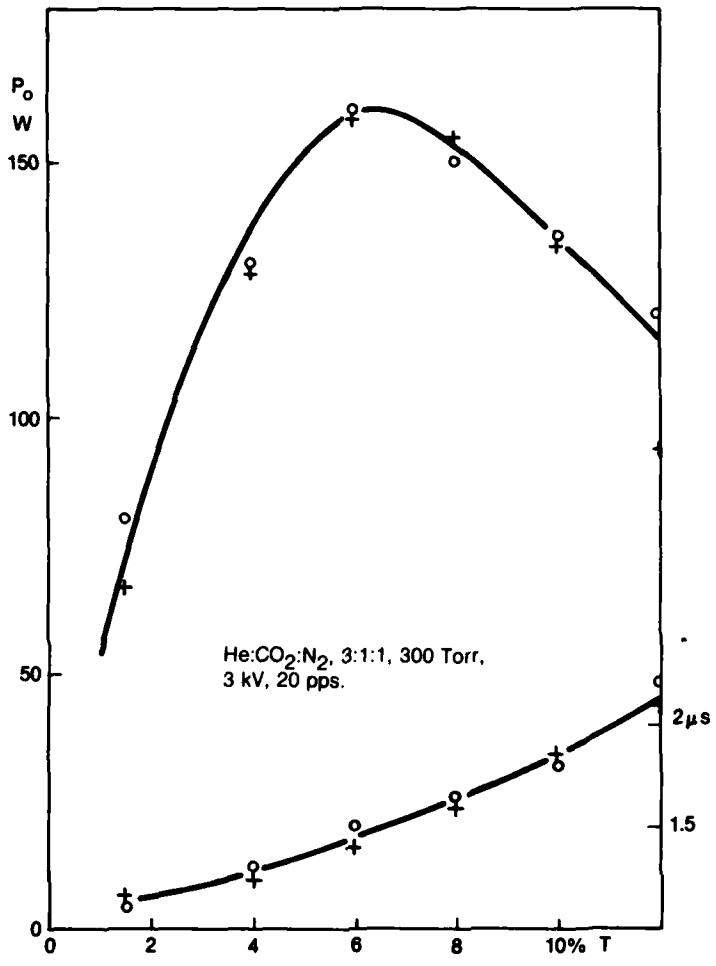

Figure 15. Power output and delay time versus mirror reflectivity: o = measured, + = computer model. (Multiply P_0 by 3.3.)

The measurements used for comparison in figure 15 were taken with a closed bore structure with a dirty bore that could not be cleaned very well. Even under these circumstances the 14-percent waveguide loss required for the computer model fit seems to be large.

Figure 17 shows that the computed, translational temperature increases less than 10 C in the time interval from the onset of the discharge current to the end of the leading laser pulse.

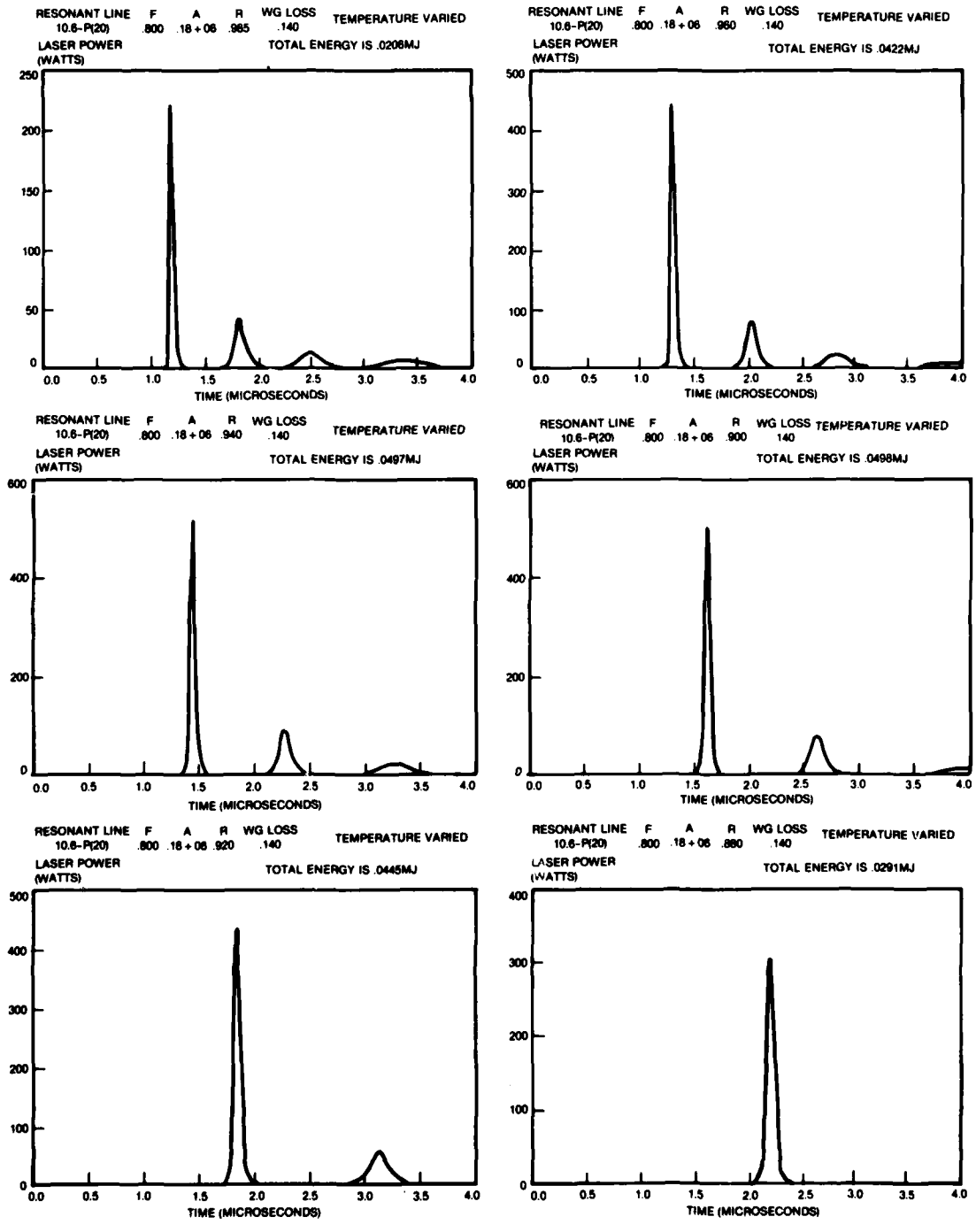

Figure 16. Output power versus time, with a mirror reflectivity as parameter.

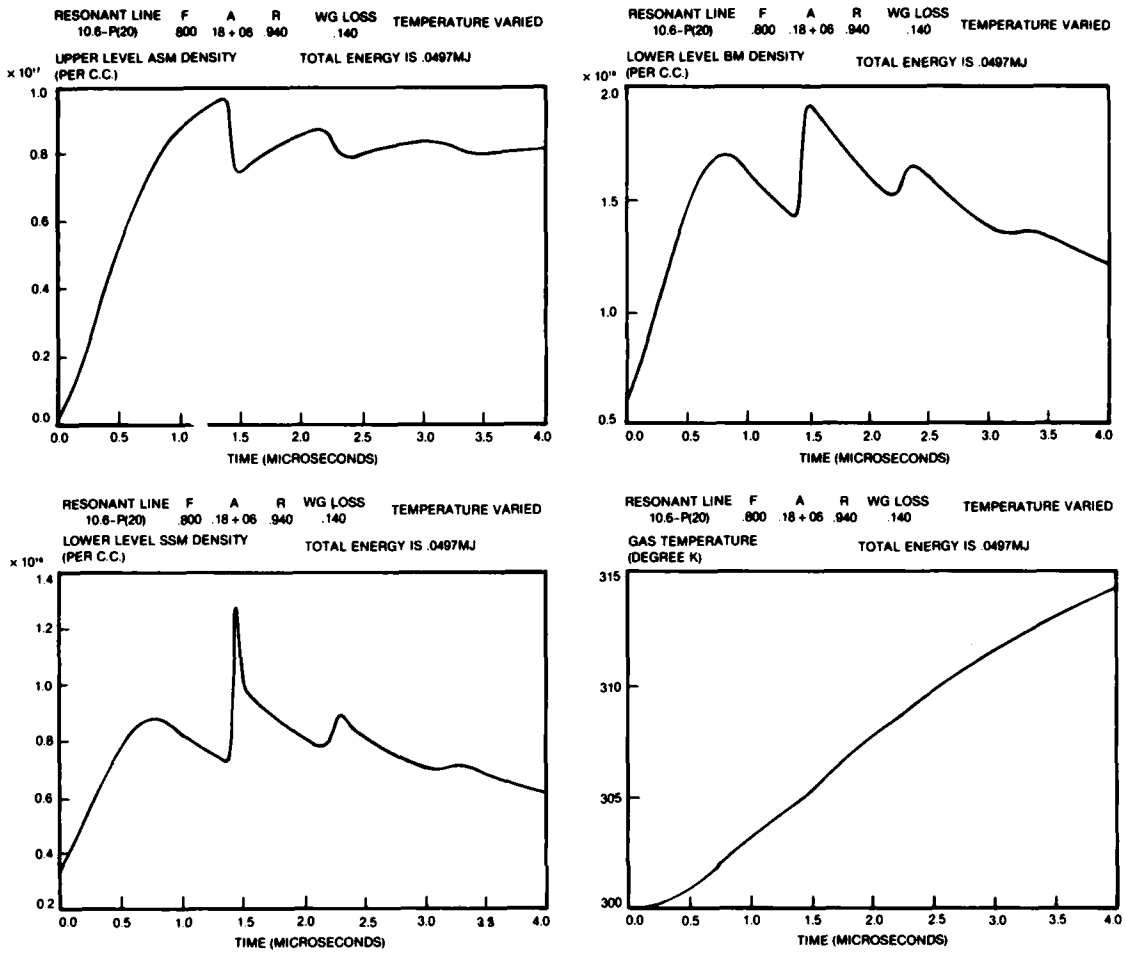

Figure 17. Level population density and translational temperature versus time.

5. CONCLUSIONS

The short, transversely excited, CO_2 gas flow waveguide laser has the potential to yield peak pulse output of 1 kW. This may require a somewhat larger bore and a better understanding of the pulse energy to peak power relationship. So far, 200-W pulses can routinely be produced and 500-W pulses can be observed under laboratory conditions. This favorable aspect of the laser can be fully exploited only if there is much more concentration on understanding and controlling the discharge conditions and the output spectrum. The present laser, delivering 1000 pulses per second, reaches its highest output 1 to 2 hours after initial

turnon. Three to six hours later, the sputtering products have increased the waveguide losses to such an extent that the power output has decreased to about 70 percent of its maximum value. Cleaning of the laser will only partially restore its original condition. The remaining electrode erosion has increased the waveguide losses, and this condition can be corrected only by replacing the electrodes as well.

We also have to mention that the instantaneous spatial distribution of the discharge conditions for the 51 electrode pairs affects the gain and can influence the mode pattern and perhaps even produce slight changes in the beam direction.

No pulse shapes have been studied far away from the laser. Since the leading pulse can contain frequency components from more than one transition, a certain amount of pulse distortion has to be expected after transmission through a dispersive medium.

Elimination of the mentioned defects will transform this type of laser into a useful and reliable device.

A far more useful type of laser for fuzing applications would be the sealed-off version, if its life could be sufficiently extended. Typical lifetime characteristics are shown in appendix A. A considerable research effort would be needed to solve the life problems associated with the sealed-off CO_2 waveguide laser to make it sufficiently reliable for fuzing applications.

LITERATURE CITED

(1) P. W. Smith, P. J. Maloney, and O. R. Wood, II, Waveguide TEA Laser, Appl. Phys. Lett. 23 (1973), 524.

(2) U. Hochuli, Properties of Small TE CO_2 Waveguide Lasers, Dept. of Electrical Engineering, University of Maryland, Technical Research Report for Contract No. DAAG30-76-C-0117, Contract report for Harry Diamond Laboratories, HDL-CR-77-117-1 (June 1977).

(3) Lee W. Casperson, Analytic Modeling of Gain-Switched Lasers, Laser Oscillators, J. Appl. Phys. 43 (1976), 4555.

(4) W. J. Witteman, On Vibrational Relaxations in Carbon Dioxide, Philips Res. Rep., Suppl. 2 (1963).

(5) K. R. Manes and H. J. Seguin, Analysis of the CO_2 TEA Laser, J. Appl. Phys. 43 (1972), 5073.

(6) D. L. Lyon, Comparison of Theory and Experiment for a Transversely Excited High-Pressure CO_2 Laser, IEEE J. Quantum Electron. QE-9 (1973), 139.

(7) W. L. Nighan, Electron Energy Distribution and Collision Rates in Electrically Excited N_2, CO, and CO_2, Phys. Rev. 2 (1970), 1989.

ACKNOWLEDGEMENTS

The author would like to thank Dr. W. L. Nighan of United Aircraft Research Laboratories for his generous loan of computer data for electron energy distributions. Some National Science Foundation funding had to be used to finish the project, and the Minta Martin fund helped to replace a damaged detector.

APPENDIX A.--SEALED-OFF OPERATION OF METAL-CERAMIC LASER

APPENDIX A

Fuzing applications require only a relatively short operating life combined with an extremely reliable and extensive shelf life. A sealed-off metal-ceramic laser structure would satisfy these requirements if the necessary operating life could be obtained. By considering the peak cathode current densities of about 40 A/cm^2, it becomes obvious that the present cathode technology, which can barely handle the 0.4 A/cm^2 required for cw operation, has to be considerably improved. Only actual experimental results can yield the life of a given laser structure under the required pulsed conditions. Besides severe electrode sputtering, we also have to expect CO_2 dissociation problems in the bore itself. Diffusion times are too long for longitudinal access to a fresh supply of gas from a reservoir outside the bore. In this respect, a structure with transverse access to an external reservoir would be far superior.

Experimental lifetimes were obtained for sealed-off operation of laser structures similar to the ones shown in figure 1 (body of report). Figure A-1 shows that a 3:1:1 $He:CO_2:N_2$ mixture yields a half power life of only 20 s for a pulse repetition rate of 30 pps. Increasing the pulse repetition rate to 200 pps reduces the life to 2 s. Figure A-2 indicates that He-rich mixtures are even more detrimental. O_2, CO, and H_2 were added to the gas mixture in an attempt to speed up the recombination of dissociated CO_2. The results, shown in figures A-3 to A-5, indicate an increased laser life. Figure A-5 shows the most favorable situation, where the addition of 6-percent H_2 increases the power output by 20 percent and the half power life to 120 s at 30 pps.

These results clearly show that the presently used, sealed-off laser structure has a very marginal life at low pulse repetition rates and a totally inadequate one at higher repetition rates. For this reason, and for the changing demand to faster pulse repetition rates, we have devoted our attention to the flow system described before.

APPENDIX A

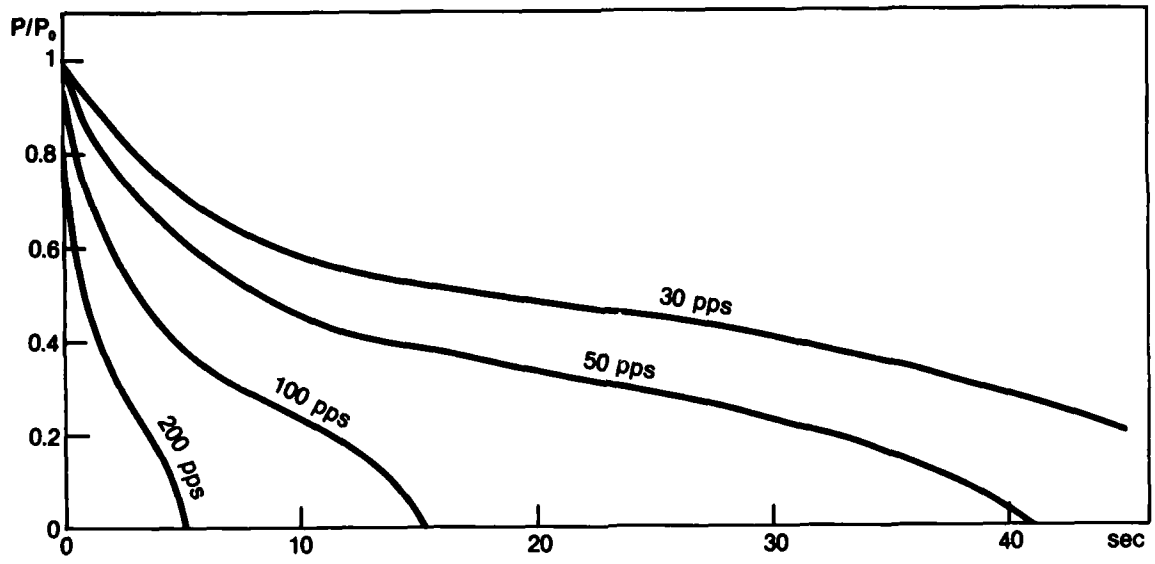

Figure A-1. CO_2 TE waveguide laser, 9.6-μm output power versus time--He:CO_2:N_2, 3:1:1; 200 Torr; 3 cc, sealed-off, 3.5 kV, 20 C.

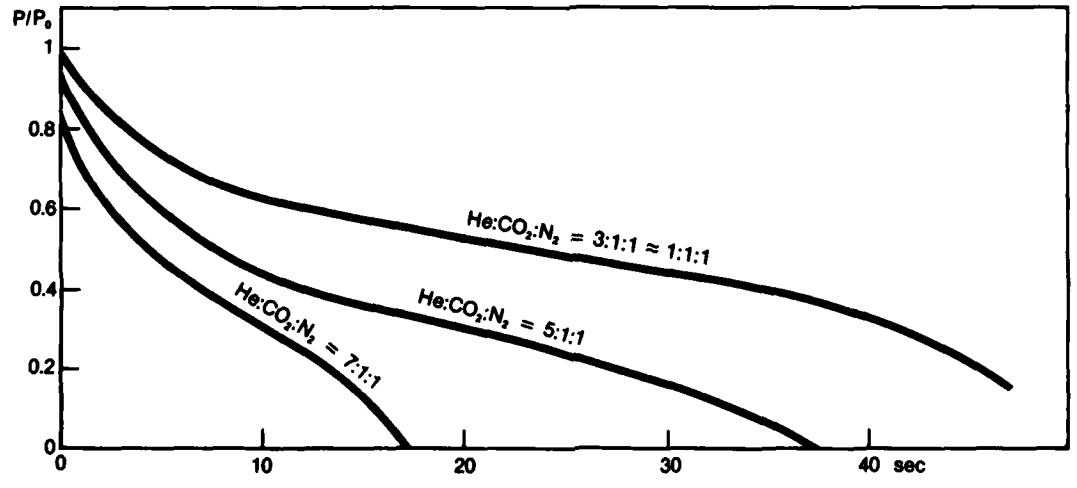

Figure A-2. CO_2 TE waveguide laser, 9.6-μm output power versus time--300 Torr, 3 cc, sealed-off, 20 C, 4 kV, 30 pps.

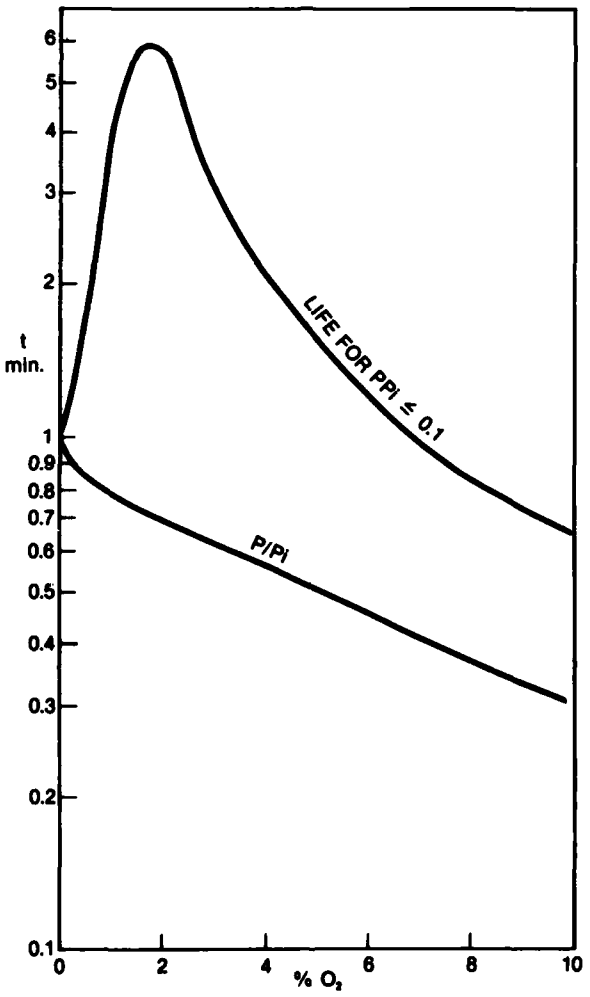

Figure A-3. CO_2 TE waveguide laser, sealed-off lifetime and 9.6-μm power output versus O_2 concentration--He:Co_2:N_2, 3:1:1; 300 Torr; 3 cc 30 pps, 4 kV, 20 C, $t(P/P_i = 0.1) \times 3t(P/Pi = 0.5)$.

APPENDIX A

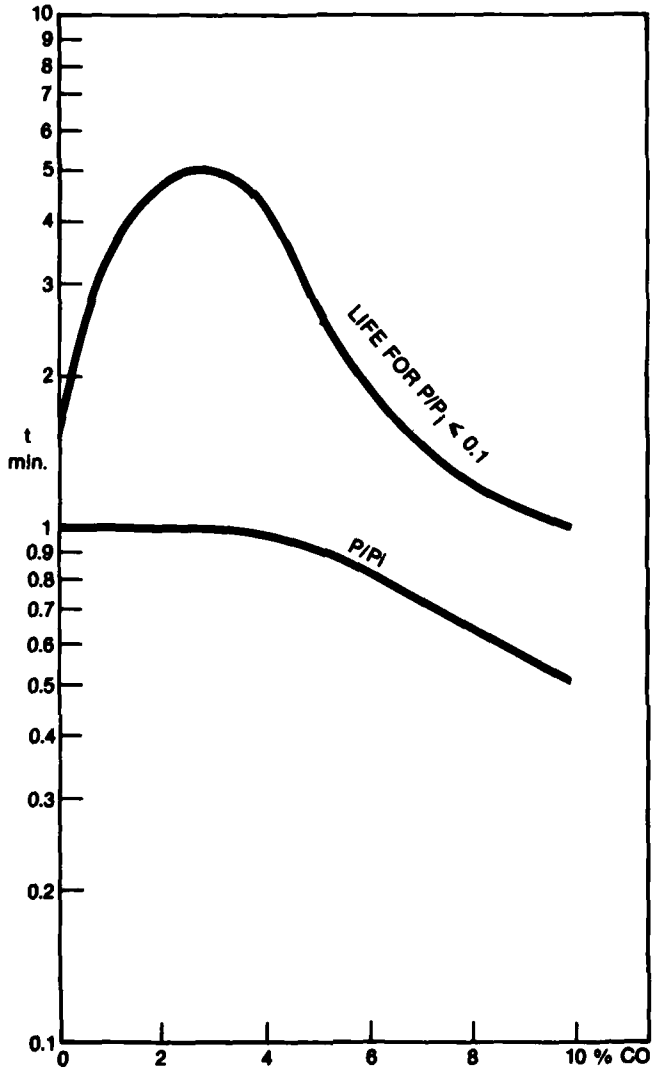

Figure A-4. CO_2 TE waveguide laser, sealed-off lifetime and 9.6-μm power output versus CO concentration--He:CO_2:N_2, 3:1:1; 300 Torr; 3 cc, 30 pps, 4 kV, 20 C, t(P/Pi = 0.1) × 3t(P/Pi = 0.5).

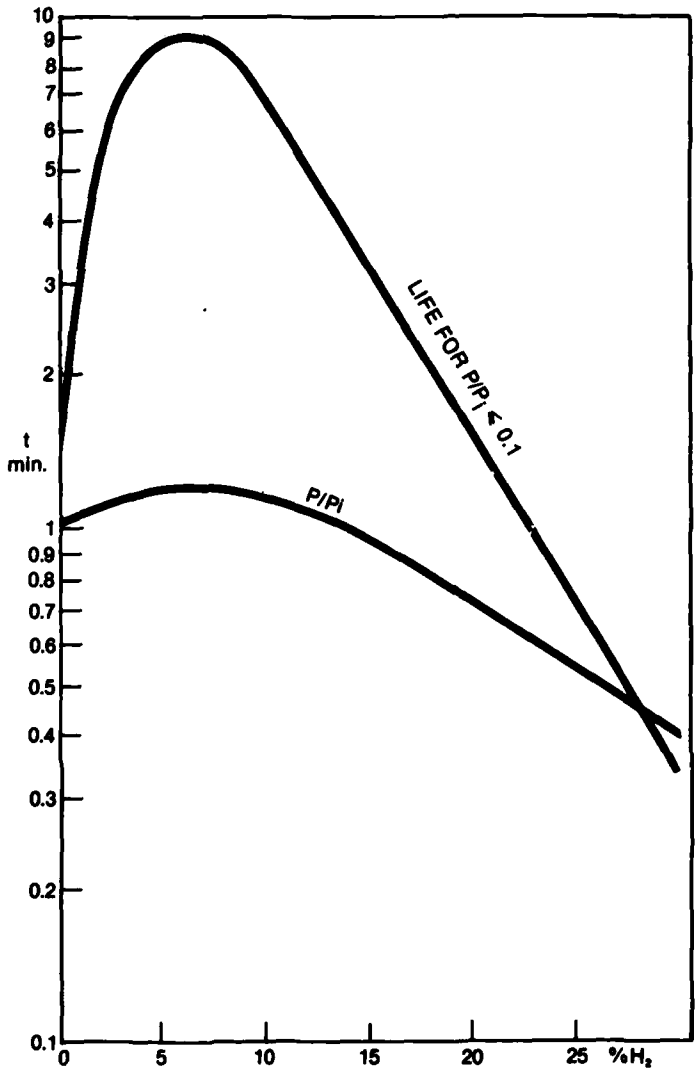

Figure A-5. CO_2 TE waveguide laser, sealed-off lifetime and 9.6-μm power output versus H_2 concentration--He:CO_2:N_2, 3:1:1; 300 Torr; 3 cc, 30 pps, 4 kV, 20 C, t(P/Pi = 0.1) ≈ 3t(P/Pi = 0.5).

DISTRIBUTION

ADMINISTRATOR
DEFENSE TECHNICAL INFORMATION CENTER
ATTN DTIC-DDA (12 COPIES)
CAMERON STATION, BUILDING 5
ALEXANDRIA, VA 22314

COMMANDER
US ARMY RSCH & STD GP (EUR)
ATTN CHIEF, PHYSICS & MATH BRANCH
FPO NEW YORK 09510

COMMANDER
US ARMY MISSILE & MUNITIONS
CENTER & SCHOOL
ATTN ATSK-CTD-F
REDSTONE ARSENAL, AL 35809

DIRECTOR
US ARMY MATERIEL SYSTEMS ANALYSIS ACTIVITY
ATTN DRXSY-MP
ABERDEEN PROVING GROUND, MD 21005

DIRECTOR
US ARMY BALLISTIC RESEARCH LABORATORY
ATTN DRDAR-TSB-S (STINFO)
ABERDEEN PROVING GROUND, MD 21005

TELEDYNE BROWN ENGINEERING
CUMMINGS RESEARCH PARK
ATTN DR. MELVIN L. PRICE, MS-44
HUNTSVILLE, AL 35807

ENGINEERING SOCIETIES LIBRARY
ATTN ACQUISITIONS DEPARTMENT
345 E. 47TH STREET
NEW YORK, NY 10017

HQ, USAF/SAMI
WASHINGTON, DC 20330

US ARMY ELECTRONICS TECHNOLOGY
& DEVICES LABORATORY
ATTN DELET-DD
FT MONMOUTH, NJ 07703

COMMANDER
US ARMY ARMAMENT RESEARCH
& DEVELOPMENT COMMAND
ATTN DRDAR-SE, SYSTEMS EVALUATION
OFFICE, LTC GRADY COOK
ATTN DRDAR-LCN-C, G. TAYLOR
ATTN DRDAR-AS, R. ANDREJZOVICS
DOVER, NJ 07801

DIRECTOR
NIGHT VISION & ELECTRO-OPTICS
LABORATORY
ATTN DELNV-V (2 COPIES)
ATTN DELNV-R, R. BUSER
FT BELVOIR, VA 22060

COMMANDER/DIRECTOR
ATMOSPHERIC SCIENCES LABORATORY
ATTN DELAS-EO, F. NILES
WHITE SANDS MISSILE RANGE, NM 88002

COMMANDER
US ARMY MISSLE COMMAND
ATTN DRSMI-REM, H. ANDERSON
REDSTONE ARSENAL, AL 35898

ENVIRONMENTAL RESEARCH INSTITUTE
OF MICHIGAN
PO BOX 8618
ATTN IRIA LIBRARY
ANN ARBOR, MI 48107

COMMANDER
NAVAL WEAPONS CENTER
ATTN CODE 3311, K. BULLOCK (4 COPIES)
ATTN CODE 3311, J. CRISLER
CHINA LAKE, CA 93555

COMMANDER
AFATL
ATTN L. STABLES
EGLIN AIR FORCE BASE, FL 32542

COMMANDER
AFAL/TEO
ATTN R. HARRIS
WRIGHT-PATTERSON AF BASE, OH 45433

MOTOROLA, INC
GOVERNMENT ELECTRONICS DIVISON
ATTN A. GARAS (2 COPIES)
PO BOX 1417
8201 E. MCDOWEL RD
SCOTTSDALE, AZ 85252

SANTA BARBARA RESEARCH CENTER
ATTN N. RIGBY (2 COPIES)
75 COROMAR DRIVE
GOLETA, CA 93117

UNIVERSITY OF MARYLAND
DEPARTMENT OF ELECTRICAL ENGINEERING
ATTN URHS HOCHULI (10 COPIES)
COLLEGE PARK, MD 20742

DISTRIBUTION (Cont'd)

US ARMY ELECTRONICS RESEARCH
& DEVELOPMENT COMMAND
ATTN TECHNICAL DIRECTOR, DRDEL-CT

HARRY DIAMOND LABORATORIES
ATTN CO/TD/TSO/DIVISION DIRECTORS
ATTN RECORD COPY, 81200
ATTN HDL LIBRARY, 81100 (2 COPIES)
ATTN HDL LIBRARY, 81100 (WOODBRIDGE)
ATTN TECHNICAL REPORTS BRANCH, 81300
ATTN CHAIRMAN, EDITORIAL COMMITTEE
ATTN LEGAL OFFICE, 97000
ATTN MORRISON, R., 13500 (GIDEP)
ATTN CHIEF, 13000
ATTN CHIEF, 11000
ATTN CHIEF, 13300
ATTN CHIEF, 11400
ATTN COX, L., 00211
ATTN HUMPHREY, R., 13300
ATTN GRIFFIN, J. R., 21100
ATTN HATTERY, W. V., 13300
ATTN SANN, K. H., 15000
ATTN PEPERONE, S., 36000
ATTN DOBRIANSKY, B., 13500 (2 COPIES)
ATTN LANHAM, C., 00213
ATTN GIGLIO, D., 15300
ATTN GEIPE, T., 22100
ATTN TUTTLE, J., 21400
ATTN VANDERWALL, J., 22800
ATTN CONNER, M., 15200
ATTN MCGUIRE, D., 13300 (10 COPIES)

END

FILMED

1-83

DTIC